Heat and Mass Transfer 39 (2003) 579–587
DOI 10.1007/s00231-002-0385-9

Numerical investigation of transient laminar natural convection of air in a tall cavity

Z.J. Zhu, H.X. Yang

Abstract Transient laminar natural convection of air in a tall cavity has been studied numerically. The Navier-Stokes and Energy equations were solved by the accurate projection method (PmIII), in which the derived Poisson equation for pressure potential was solved by the approximate factorization one method (AF1). The aspect ratio of the tall cavity is 16, and the Prandtl number of air filled in the tall cavity is 0.71. To obtain the numerical results of heat transfer by natural convection of air in the tall cavity, the second order schemes for the space and time discretizations were utilized. The availability of the numerical algorithm was also assessed by considering the natural convection of air in a square cavity which is differentially heated from side walls. It was found that the overall Nusselt numbers for the Rayleigh numbers covering the range from 1000 to 100000 reveal a good agreement with measured data. When Ra takes the value in the range from 100000 to 600000, the overall Nusselt number have a relative deviation less than 18% from the experimental data. For the suddenly heating mode, the multicellular flow pattern occurs when Rayleigh number belongs to the range of Ra from 7000 to 20000. or greater than 115000. At the critical number of cats' eye instability, the cell distance is just twice of the cavity width. This is rather similar to the observed result for Bénard problem. When Ra is over 115000, a further increase of heat flux across the tall cavity causes serious cell-breaking. There are 8 cells when Ra = 600000.

Received: 1 October 2001
Published online: 31 October 2002

Z.J. Zhu (✉)
The State Key Laboratory of Fire Science,
Department of Thermal Science and Energy Engineering,
University of Science and Technology of China,
Hefei, Anhui 230026, P.R. China
E-mail: zuojin@ustc.edu.cn
Tel.: 86-551-3603803
Fax: 86-551-3631760

H.X. Yang
Department of Building Services Engineering,
The Hong Kong Polytechnic University,
Hung Hom, Kowloon, Hong Kong

Financial support from the State Key Laboratory of Fire Science and the Earmarked Research Project with Grant No. B-Q373

Nomenclature

A	$=L/H$, aspect ratio of the tall cavity
E_{av}	overall kinetic energy
g	gravitational acceleration, m/s^2
H	cavity width, m
I	grid number in z-direction
J	grid number in y-direction
κ	thermal conductivity W/mK
L	cavity height, m
n	unit normal vector of a boundary surface m
N_c	number of cells
p	pressure Pa
Pr	Prandtl number
Ra	$= g\beta_T(T_h - T_c)H^3/\nu\kappa$ Rayleigh number
Nu_{av}	average Nusselt number
T_h	temperature of the hot wall K
T_c	temperature of the cold wall K
u*	variable in accurate projection defined m/s
u	$= (v, w)$, velocity vector m/s
v	velocity component in y-direction m/s
w	velocity component in z-direction m/s
w_0	reference velocity m/s

Greek symbols

β_T	coefficient of fluid thermal expansion, 1/K
χ	pressure potential
Δt	non-dimensional time interval
ΔT	$= T_h - T_c$, temperature difference K
Ω	Domain of numerical simulation
$\partial\Omega$	Domain boundaries
ψ	Stream function
Θ	non-dimensional temperature
ρ	density of fluid, kg/m^3
∇^2	Laplacian operator

Superscript

n	time level

Subscript

T	Thermal

1
Introduction

The heat transfer problem of natural convection in a tall cavity has been considered by many researchers for a century, owing to its great importance in solar energy and building services engineering systems, and other engineering systems as well. A literature review before 1988 was given by Ostrach [1]. The early works were primarily conducted by theoretical analysis and experiments. It is well known that Batchelor [2] first noticed that natural convective flow regime in a tall cavity at small Rayleigh numbers. It was shown that in a differentially heated cavity, fluid flows along the heated wall, and turns in the top end, then sinks along the cold wall, and turns again in the bottom end. However, in the central portion of the tall cavity, the vertical velocity holds a cubic profile, and the temperature decreases linearly from the temperature of the hot wall to that of the cold wall.

Remembering this picture described by Batchelor, and considering the visual observations and experimental measurements given for the same regime by Elder [3], Gill [4] developed a well known theory for this problem on boundary-layer regime in 1966, in which the top and bottom walls are adiabatic. The fundamental assumption was that a stratified fluid core exists far away from both vertical walls, which was taken as the matching accordance of the boundary-layer solutions for flows near the vertical walls. Considering the impermeable and adiabatic properties of the horizontal end walls, Bejan [5] further proposed an alternative approach to evaluate the arbitray constants appeared in Gill's solution for the boundary-layer natural convection regime in a tall cavity. This approach was used by Graebel [6] to consider the effects of Prandtl number on the natural convection in a rectangular cavity. By using a modified Oseen technique, it was found that a midsection shear layer develops for a Prandtl number less than 1/7.

Ostrach and Raghavan [7] have investigated the effect of stablizing thermal gradients on natural convection in rectangular enclosures when the Prandtl numbers of fluids were of order 10^5, Grashof numbers ranged up to 20, and the aspect ratios were 1 and 3. ElSherbiny et al. [8] have carried out their important experimental work on natural convection in vertical and inclined air layers. Detailed results were reported by figures and data correlations as well. Hollands and Konicek [9] have determined experimentally the critical Rayleigh number for differentially heated inclined air layers. The principle of the experimental method was first reported by Schmidt and Milverton [10], which was adopted to study the Bénard problem experimentally.

With the development of computer science and technology, numerical simulation has played an important role in many fields including that of thermal science. As a matter of fact, the numerical studies on the onset of layered convection in a narrow slot containing a stably stratified fluid has been reported by Wirtz and Liu [11] at the end of 1970s. The calculation agreed generally with the experimental data of Hart [12], and the evolution of overall kinetic energy was given graphically. Korpela and his coworkers [13] have carried out numerical studies on heat transfer through a double pane window.

However, more interestingly, Le Quéré [14] has reported the multiple and unsteady numerical solutions of two dimensional natural convection in a tall cavity, in which the space discretization for the governing equations was based on the Chebyshev expansions. Further, the accuracy of time integration was improved to third order, greater than the usually used second order, which was accomplished by combining a backward Euler scheme for the diffusive terms with an explicit extrapolation for the convective terms by Adams-Bashforth scheme. It was found that several braches of solutions characterized by different numbers of cells in the flow field, and the return to the unicellular flow structure occur through a gradual decrease in the number of cells. As reported, each changes in the number of cells is characterized by hysteresis. However, it should be noted that even though the results do convey an amazing insight of natural convection in a tall cavity, but the grid used in the numerical study seems to be too coarse at present time. Thus, further study is required for the deep understanding of the transition of flow patterns occurred under the conditions of Rayleigh number near or larger than the corresponding critical value.

Recently Jin and Chen [15] have reported the numerical results of instability of natural convection and heat transfer in case of large Prandtl number of fluids in a vertical slot with an attempt to compare with the experimental results given by Wakitani [16]. Similar to numerical solutions of Le Quéré, Wakitani [17] has reported the development of multicellular patterns found in the natural convection in an air-filled tall cavity.

We have studied the thermal induced flow instability in a horizontal parallel plate channel numerically by using a fractional algorithm [18]. The corresponding experimental visualization have been reported by Lir and Lin [19]. In this paper, we focus our attentions on the natural convection in a tall cavity filled with air. The thermal induced convective flow patterns, and the evolution of flow field as well as the overall Nusselt number are obtained by direct numerical solution of the governing equations with PmIII, which is an accurate projection method developed by Brown et al. [20]. The schematic of the tall cavity with respect ratio $A(=L/H)$ is illustrated in Figure 1. The cavity is heated from the left vertical wall whose temperature is higher than that of the right vertical wall with a constant temperature difference ΔT $(=T_h - T_c)$. The implementation of PmIII shows that it is stable, and the numerical results obtained were found to be consistent with those existed experimental results.

2
Governing equations and numerical method

2.1
Governing equations

Consider the laminar natural convection happened in a tall cavity schematically shown in Figure 1, where fluid filled with kinematic viscosity ν and thermal diffusivity κ is induced to flow upward due to the heat transfer from the left wall with temperature T_h, and the initial temperature

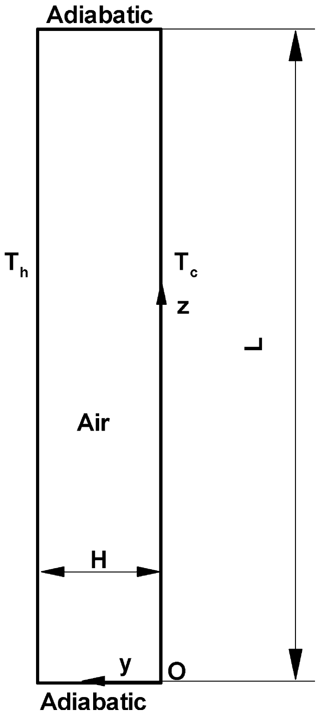

Fig. 1. The schematic diagram of the tall air cavity heated differentially

of fluid is the same as that of the right walls T_c. The horizontal end side walls are adiabatic. The two dimensional system given in Figure 1, where the coordinate Oz has an opposite direction of gravity **g**. Similar to Wakitani [17], we introduce $w_0 = \sqrt{(g\beta_T H \Delta T)}$ to measure velocity, taking H as the measure of length, and $t_0 = H/w_0 = \sqrt{(Pr/Ra)}H^2/\nu$ as the measure of time. Thus, if we choose $\rho {w_0}^2$ as the measure of pressure, define $\Theta = (T - (T_c + T_h)/2)/\Delta T$, and assume that the Boussinesq approximation holds, the dimensionless governing equations for the heat transfer problem are:

$$\frac{\partial \Theta}{\partial t} + \frac{\partial v\Theta}{\partial y} + \frac{\partial w\Theta}{\partial z} = \frac{1}{\sqrt{RaPr}} \nabla^2 \Theta \tag{1}$$

$$\frac{\partial v}{\partial y} + \frac{\partial w}{\partial z} = 0 \tag{2}$$

$$\frac{\partial v}{\partial t} + \frac{\partial vv}{\partial y} + \frac{\partial wv}{\partial z} = -\frac{\partial p}{\partial y} + \left(\frac{Pr}{Ra}\right)^{\frac{1}{2}} \nabla^2 v \tag{3}$$

$$\frac{\partial w}{\partial t} + \frac{\partial vw}{\partial y} + \frac{\partial ww}{\partial z} = -\frac{\partial p}{\partial z} + \Theta + \left(\frac{Pr}{Ra}\right)^{\frac{1}{2}} \nabla^2 w \tag{4}$$

whose alternative forms are

$$\Theta_t + (\mathbf{u} \cdot \nabla)\Theta = (1/PrRa)^{\frac{1}{2}} \nabla^2 \Theta \tag{5}$$

and

$$\nabla \cdot \mathbf{u} = 0 \tag{6}$$

$$\mathbf{u}_t + (\mathbf{u} \cdot \nabla)\mathbf{u} = -\nabla p + \Theta\lambda + (Pr/Ra)^{\frac{1}{2}} \nabla^2 \mathbf{u} \tag{7}$$

where $\lambda = (0, 1)$ is the unit vector in the vertical direction, and Pr is the Prandtl number accompanied by the Rayleigh number $Ra = g\beta_T(T_h\ T_c)H^3/\nu\kappa$.

The solutions of the governing equations (5)–(7) should be sought under appropriate conditions which are compatible with the problem considered. As aforementioned, the boundary conditions on the two vertical walls can be written as

$$v = 0, \quad w = 0, \quad \Theta = 0.5, \quad \text{for } y = 1 \tag{8}$$

and

$$v = 0, \quad w = 0, \quad \Theta = -0.5, \quad \text{for } y = 0 \tag{9}$$

For the horizontal side walls, we have

$$v = 0, \quad w = 0, \quad \partial\Theta/\partial z = 0, \quad \text{for } z = 0, \text{ or } A \tag{10}$$

On the other hand, the initial conditions are simply assigned as

$$v = 0, \quad w = 0, \quad \Theta = 0, \quad \text{in } \Omega, \text{ when } t = 0 \tag{11}$$

2.2
Numerical method

The accurate projection method developed by Brown et al. (2001) employs two new variables, $\mathbf{u}^*$ and χ, which have the relation to the velocity vector as below

$$\mathbf{u}^* = \mathbf{u} + \nabla\chi \tag{12}$$

where χ is the potential, and $\mathbf{u}^*$ is the intermediate velocity vector. Let Ω represent the domain with boundary $\partial\Omega$, in which the projection is

$$\mathbf{u} = \mathbf{P}(\mathbf{u}^*) \tag{13}$$

where **P** is the Projection operator. With the new variables, the evolution equation becomes

$$\mathbf{u}_t + (\mathbf{u} \cdot \nabla)\mathbf{u} + \nabla\chi_t = \frac{1}{2}\sqrt{Pr/Ra}\nabla^2[\nabla\chi + 2\mathbf{u}] \tag{14}$$

$$\mathbf{u}|_{\partial\Omega} = \mathbf{u}_b \tag{15}$$

Equations (12)–(15) constitute an equivalent formulation of the Navier-Stokes equations (2)–(4). In this formation the relevant pressure potential χ takes the place of pressure p, which can be recovered from the potential χ by stressing the corresponding equivalence aforementioned, that is

$$p = \left(\frac{\partial}{\partial t} - \frac{1}{2}\sqrt{Pr/Ra}\nabla^2\right)\chi \tag{16}$$

Note that a Poisson problem is solved in the numerical implementation of the projection method. A standard five-point stencil approximating to the Laplacian and second-order central differences for divergence and gradient were generally used. Accordingly, this combination actually

Table 1. Detail Comparison of the Calculation Results for $A = 1$ in cases of 65×65[†]

Ra	10^5		10^6		10^7	
$\psi_{\frac{1}{2}\frac{1}{2}}$	9.119	9.109	16.39	16.46	29.27	30.10
ψ_{max}	9.619	9.602	16.811	16.845	30.17	30.74
$\frac{1-y}{z}$	$\frac{0.285}{0.601}$	$\frac{0.294}{0.611}$	$\frac{0.151}{0.548}$	$\frac{0.148}{0.548}$	$\frac{0.086}{0.556}$	$\frac{0.087}{0.548}$
v_{max}	34.75	44.22	64.83	135.34	148.8	446.97
z	0.855	0.897	0.850	0.944	0.879	0.964
w_{max}	68.64	68.42	220.06	222.22	699.3	716.84
$1 - y$	0.066	0.071	0.0375	0.0397	0.0213	0.0238
$Nu_{\frac{1}{2}}$	4.523	4.643	8.826	8.286	16.51	14.42
Nu_{av}	4.522	4.506	8.825	8.703	16.52	16.255
Nu_{max}	7.720	7.671	17.536	17.296	39.37	39.459
z	0.082	0.0714	0.039	0.0397	0.018	0.0238
Nu_{min}	0.728	0.749	0.979	1.052	1.367	1.513
z	1	1	1	1	1	1

[†]For a given Ra, the values in the left column was abstracted from Ref. [24] (Le Quéré, 1985)

provides an approximate projection operator which means that the projected velocities only satisfy a discrete divergence constraint to a truncation error. The time-discrete forms of PmIII for the solution of the governing equations are:

$$\frac{\Theta^{n+1} - \Theta^n}{\Delta t} = -[(\mathbf{u} \cdot \nabla\Theta)]^{n+\frac{1}{2}} + \frac{1}{2}\left(\frac{1}{RaPr}\right)^{\frac{1}{2}} \nabla^2(\Theta^{n+1} + \Theta^n) \tag{17}$$

$$\frac{\mathbf{u}^{*n+1} - \mathbf{u}^n}{\Delta t} = -\left[(\mathbf{u} \cdot \nabla\mathbf{u})\right]^{n+\frac{1}{2}} + \left[\Theta\right]^{n+\frac{1}{2}}\lambda + \frac{1}{2}\left(\frac{Pr}{Ra}\right)^{\frac{1}{2}} \nabla^2(\mathbf{u}^{*n+1} + \mathbf{u}^n) \tag{18}$$

$$\mathbf{u}^{n+1} = \mathbf{u}^{*n+1} - \nabla\chi^{n+1} \tag{19}$$

and

$$p^{n+\frac{1}{2}} = \frac{\chi^{n+1} - \chi^n}{\Delta t} - \frac{1}{2}\left(\frac{Pr}{Ra}\right)^{\frac{1}{2}} \nabla^2(\chi^{n+1} + \chi^n) \tag{20}$$

where χ satisfies the Poisson's equation

$$\nabla^2\chi = \nabla \cdot \mathbf{u}^* \tag{21}$$

whose boundary conditions are given by

$$\hat{\mathbf{n}} \cdot \mathbf{u}^* = \hat{\mathbf{n}} \cdot \mathbf{u}_b, \quad \hat{\tau} \cdot \mathbf{u}^* = \hat{\tau} \cdot (\nabla\chi + \mathbf{u}_b) \quad \text{on } \partial\Omega \tag{22}$$

Thus

$$\hat{\mathbf{n}} \cdot \nabla\chi = 0 \quad \text{on } \partial\Omega \tag{23}$$

The convective terms in the time discrete form were evaluated by the second order Adams-Bashforth formula. The second order upwind scheme was used in space difference. Θ and $\mathbf{u}$ were calculated by using the second order Crank-Nicolson method. The pressure potential χ was calculated by the procedure following reference [21], where the approximate factorization I method, AF1, is described in detail for approximating Laplacian operator by Baker [22]. Iterations based on AF1 have a history of quick convergence with the solutions having high accuracy as shown by a comparison made for a benchmark problem (see Ref. [21]).

The pressure field can be obtained from the potential field χ if necessary. From the calculated $\mathbf{m}^{m+1}$ and the potential χ, we have

$$\mathbf{u}^{n+1} = \mathbf{u}^{*n+1} - \Delta t \nabla\chi^{n+1} \tag{24}$$

The PmIII can also provide second order accuracy for pressure even at grids near the boundaries, and this seems to be the main potentiality over those frequently used in previous work, such as those of Kim and Moin [23]. The choice of Δt needs to fulfill the numerical stability condition, i.e. the Courant number should be less than unity since the method for the governing equations of natural convection in the tall cavity is semi-implicit.

2.3 Method assessment

The numerical method given in the foregoing subsection was assessed by considering the natural convection of air in a square cavity. The upper and lower walls of the cavity were insulated perfectly, and the values of normalized temperature Θ for the left and right vertical walls were assigned as 0.5 and –0.5 respectively. The initial value of temperature Θ in the cavity was zero. To verify the numerical method carefully and rigorously, the computational results for the benchmark problem obtained by using $\Delta t = 8 \times 10^{-3}$ and saved at $t = 200$ were given in Table 1, where the numerical results given in reference [24] (Le Quéré, 1985) were abstracted for comparison. It was viewed that in addition to the horizontal component of velocity v, whose value given by present method is larger than that reported in Ref. [24], there is a satisfactory agreement between the numerical results provided by the two kinds of different numerical algorithm. It was confirmed that using the horizontal velocity component v which was calculated by current method can also provide the same field of stream function as that obtained by appreciating vertical velocity component w. The temperature and flow fields for $Ra = 10^7$ are shown in Figure 2. Again, it was viewed that these contours are in good consistent with those given in reference [24]. To confirm the arrival of steady field for the natural convection in case of $Ra = 10^7$, the evolution of the overall Nusselt number was shown in Figure 3 (a), while the distribution of local Nusselt number along the left vertical wall was illustrated in Figure 3 (b). Therefore, it can be concluded that the numerical method

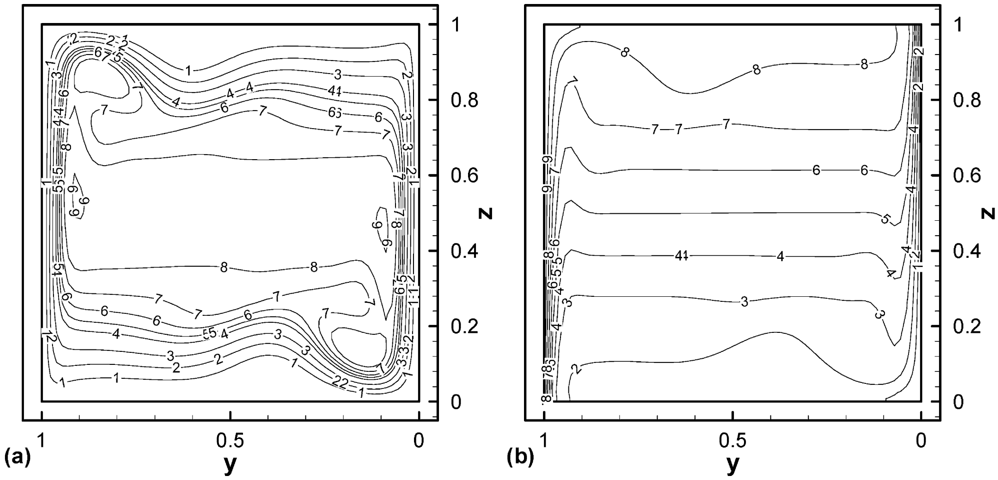

Fig. 2. Flow and temperature fields for $Ra = 10^7$ and grid 65 × 65 when $t = 200$. (a) Streamlines labeled by 1, 2, …, 8, 9 are corresponding to $\psi^{\dagger}(= \psi\sqrt{Ra\,Pr})$ values: 5, 10, 15, 20, 22, 24, 26, 28, 30.5. (b) Isotherms labeled by 1, 2, …, 8, 9 are corresponding to Θ values −0.4, via 0, to 0.4 with an increment 0.1

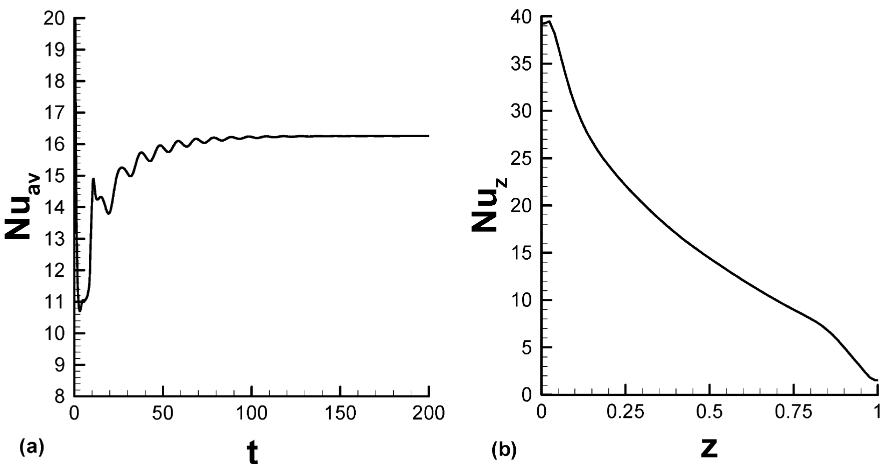

Fig. 3. (a) The evolution of overall Nusselt number for $Ra = 10^7$, and cavity ratio $A = 1$; and (b) The distribution of local Nusselt number along the left side vertical wall for the same Rayleigh number and cavity ratio when $t = 200$

Table 2. The Grid Dependence of Numerical Results for $Ra = 11000$

Grid	ψ^* (0.5, 8)	Nu_{av}
121 × 25	38.492	1.523
241 × 49	38.193	1.525
301 × 61	38.216	1.525

PmIII is applicable to the study of natural convection of air in a cavity.

To show the grid-independence of numerical results for the problem on hand, a test was conducted for $Ra = 11000$, and the corresponding results were given in Table 2. It was found that as soon as the gird is finer than 241 × 49, the overall Nusselt number calculated numerically remains the same. This implies that the grid 241 × 49, or other finer alternatives, can be utilized in the numerical treatment of current problem.

3
Results and discussion

Since the aspect ratio of the tall cavity was given by $A = 16$, the width of the cavity H was taken as 0.03m with the height $L = AH = 0.48$ m. Nearly uniform space grid systems was used, where, for a grid node near a wall, the distance from the node to the wall were taken as half of the mesh size Δx or Δz for internal grid nodes. The time interval Δt was taken as 0.004. The Prandtl number of air under atmospheric pressure was 0.71, but for the current numerical study, the range of Rayleigh number was chosen from 10^3 to 6×10^5. The numerical investigation was carried out in a Pentium II type personal computer whose primary frequency is 350 MHz.

The Poisson equation for potential χ was solved by the iterative algorithm called approximate factorization one AF1. The criteria of iteration is that the relative error defined by $\epsilon = \|\delta p^k\|/(10^{-4} + \|p^k\|)$ should be less than 10^{-4}, here k denotes the iteration level, and the iterative increment δp^k is given by $(p^k - p^{k-1})$.

3.1
Multicellular flow patterns

Owing to the onset of flow instability, the natural convection manifests multicellular patterns dominated by Rayleigh number and Prandtl number.

Figure 4 conveys the steady temperature and flow fields shown by isotherms and streamlines for $Ra = 7000$, which were obtained by starting from a uniform initial stationary state. The cats' eye structure including four cells does emerge, and this is quite similar to the pattern given in reference [24]. The cellular structure reveals its negative symmetry with respect to the central point of the cavity (0.5, 8). It should be noted that the cell distance is 2.0 in

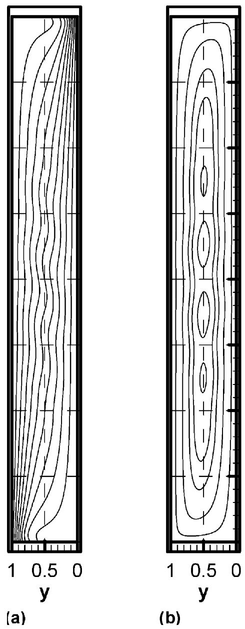

Fig. 4. The temperature and flow fields for Ra = 7000 and grid 301 × 61 when t = 200. (a) The isotherms for Θ values given by –0.4, –0.3, …, 0.3, 0.4 with an increment 0.1; (b) The streamlines for values of $\psi^*(=\psi\sqrt{Ra/Pr})$ given by 2, 9, 16, 20, and 24

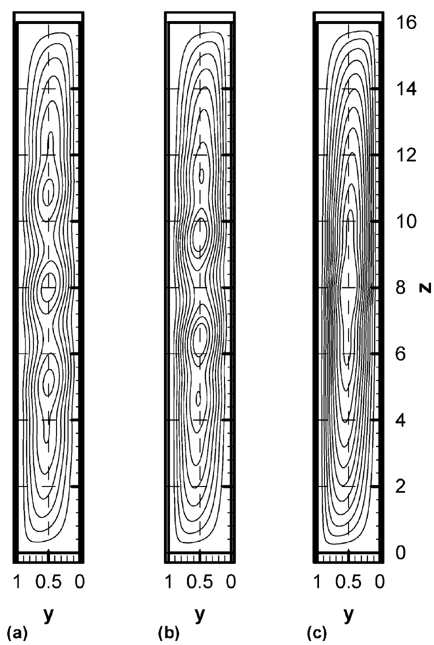

Fig. 5. The flow fields for grid 301 × 61 when t = 200 and (a) Ra = 11000, and $\psi^*(=\psi\sqrt{Ra/Pr})$ = 5, 10, 15, 20, 25, 30, and 35; (b) Ra =14000, and ψ^* = 5, 10, 15, 20, 25, 30, 35, 40, and 44; (c) Ra = 20500, and ψ^* = 5, 10, 15, 20, 25, 30, 35, 40, 45, 50, and 54

the case of Ra = 7000. This is different from the value (2.817) obtained by Le Quéré (1990), see Ref [24], however, the current cell distance is coincident with the experimental result for Bénard problem, for which it was found that the width of cells is about twice the depth of the horizontal layer (see Ref. [25], Chandrasekhar, 1961). In addition, the reason of regarding the fields saved at t = 200 as steady state of natural convection is that, from Figure 9,

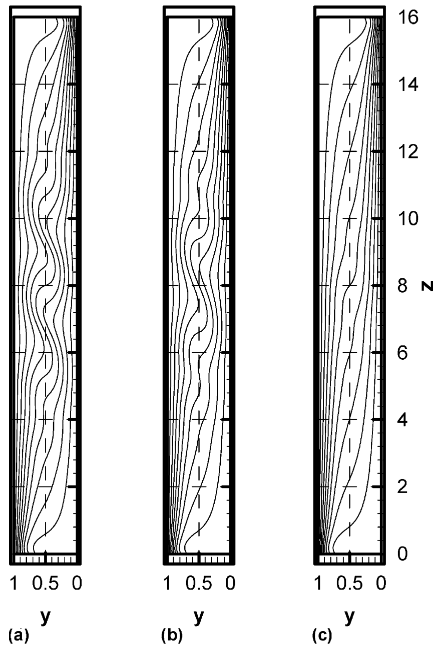

Fig. 6. The temperature fields for grid 301 × 61 when t = 200. Where, for Ra = 11000, 14000, and 20500, the isotherms for values of Θ changed from –0.4 via 0 to 0.4 with an increment 0.1 are shown in (a), (b) and (c), respectively

Table 3. The Number of Cells for different values of Ra

$Ra \times 10^{-3}$	N_c	$Ra \times 10^{-3}$	N_c	$Ra \times 10^{-3}$	N_c
7	4	14	4	118	3
9	5	18	4	150	4
10	3	20	2	200	4
11	3	20.5	1	450	7
12	4	115	1	600	8

Table 4. The Overall Nusselt Numbers for Different Ra

Ra	Nu_{av}	$Nu_{av,\ exp}$*	Ra	Nu_{av}	$Nu_{av,\ exp}$
1000	1.029	1.03	40000	2.226	2.286
3000	1.131	1.121	50000	2.370	2.450
5000	1.234	1.297	70000	2.601	2.720
7000	1.335	1.405	90000	2.765	2.941
10000	1.484	1.502	150000	3.124	3.447
11000	1.525	1.544	200000	3.357	3.771
14000	1.636	1.685	300000	3.723	4.279
20000	1.806	1.847	600000	4.356	5.313

*Interpolated value from the correlations labeled ($A2$) and ($A3$) in Ref. [8]

one can find that the overall Nusselt number has remained to be constant for a long time.

The dominating feature of Rayleigh number on the multicellular pattern can be found clearly from Figure 5, where the contours of stream function for Ra = 11000, 14000, and 20500 are illustrated. The corresponding value of stream function was enlarged by a factor $\sqrt{Ra/Pr}$ to provide the convenience of comparison with published results. For Ra = 20500 there is only one cell. However, for Ra = 11000 and 14000 there are 3 and 4 cells. But to say

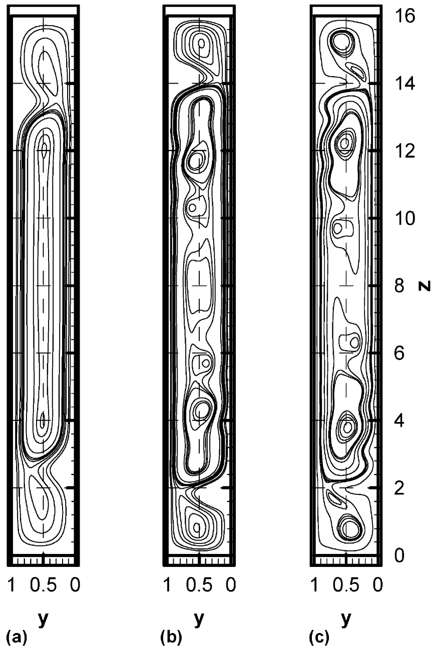

Fig. 7. The flow fields for grid 241 × 49 when t = 200 and (a) Ra = 150000, and $\psi^*(=\psi\sqrt{Ra/Pr})$ = 20, 30, 50, 60, 70, 75, 80, 100, 130, 140, and 145; (b) Ra =450000, and ψ^* = 20, 30, 50, 60, 70, 75, 80, 100, 160, 170, 175, 180, 200, 210, and 215; (c) Ra = 600000, and ψ = 20, 60, 70, 72, 75, 80, 120, 150, 180, 190, 195, 240, 250, 260, and 275

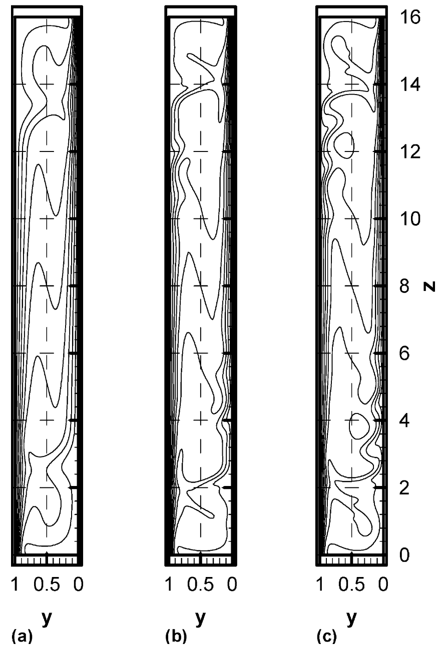

Fig. 8. The temperature fields for grid 241 × 49 when t = 200. Where, for Ra = 150000, 450000, and 600000, the isotherms for values of Θ changed from −0.4 via 0 to 0.4 with an increment 0.1. are shown in (a), (b) and (c), respectively

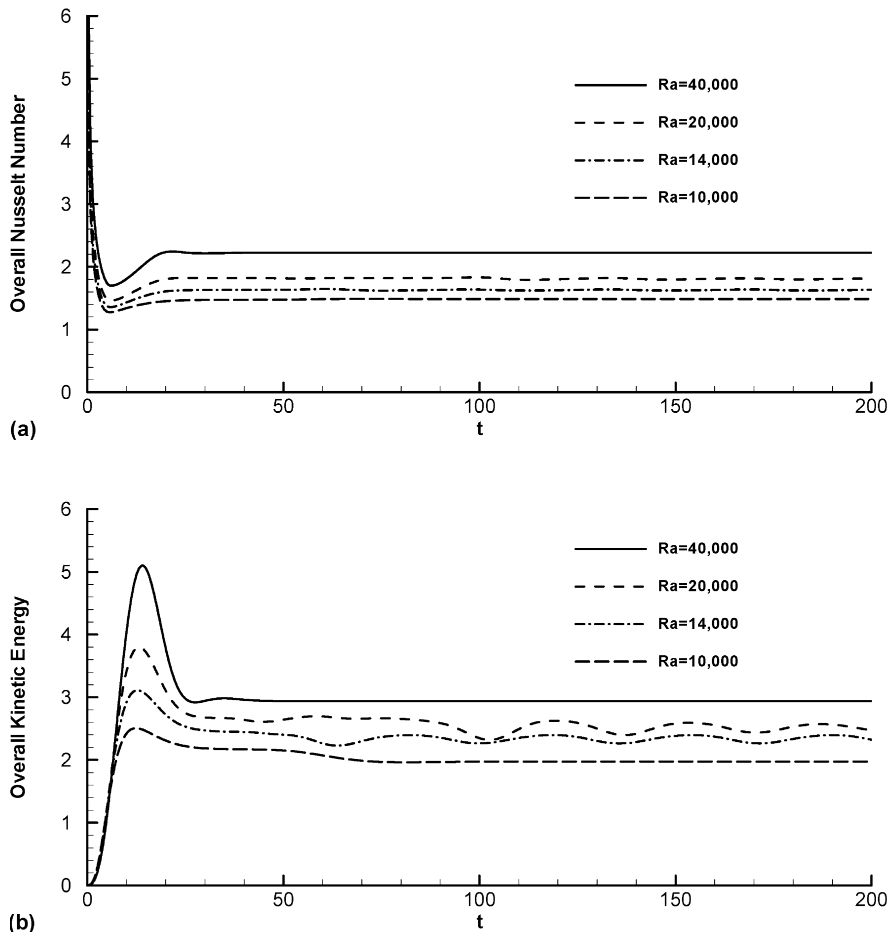

Fig. 9. The evolution of (a) overall Nusselt numbers Nu_{av}; and (b) The overall kinetic energy E_{av} for several values of Ra

that there are 4 cells appears in case of Ra = 14000 would be a forced analogy, since the two cells accompanying the two large cells in the central region are rather small and weak. The cell distance for Ra = 11000 is 2.893. But for Ra = 14000 it is 3.073. The cell distance for the pair of large and small cells closed mutually is just 2.0. The relation of cell number to Rayleigh number is again illustrated in Table 3. The cellular pattern determines the characteristics of isotherms shown in Figure 6, where the relevant Θ values are changed from –0.4, via 0 to +0.4. From Figure 6, it was seen that in the flow region where the cells are present, there are little background thermal stratification in the flow. This is in good consistent with the result reported in references [13] (Korpela et al. 1982).

Further increasing Rayleigh number, and conducting numerical simulation of the problem considered, it was found that the cell numbers increased as Rayleigh number beyond 150000. This can be observed from Figure 7 which shows that too large heat flux leads to cellular decomposition when $Ra \geq 15000$. Figure 8 shows the corresponding isotherms, from which the intrinsic property of negative symmetry can also be observed. There are 4, 7, and 8 cells for the three values of Ra, The shape of cells has been deformed and have become far different from the shape of those emerged at lower Rayleigh number. These cells cause the effect of isotherm-stretching, and this can be seen from Figure 8 (a), (b) and (c).

3.2
Nusselt number and kinetic energy

The time variation of overall Nusselt numbers ($Nu_{av} = -1/A \int_0^A \partial\Theta/\partial y \, dz$) for several values of Ra beyond the critical Rayleigh number (about 7000) is shown in Figure 9 (a), while the overall kinetic energy ($E_{av} = 1/2 \int_0^A \int_0^1 (v^2 + w^2) dy \, dz$) is illustrated in Figure 9 (b). The overall Nusselt numbers for each Rayleigh number drop quickly at the initial time period, via its *minima*, then increase to a steady state. In the time period, the overall Nusselt number changes significantly. But this is really a small percent of the gross time range, say about 10%. Similarly, in the initial time period, the overall kinetic energy E_{av} also emerge evident variation.

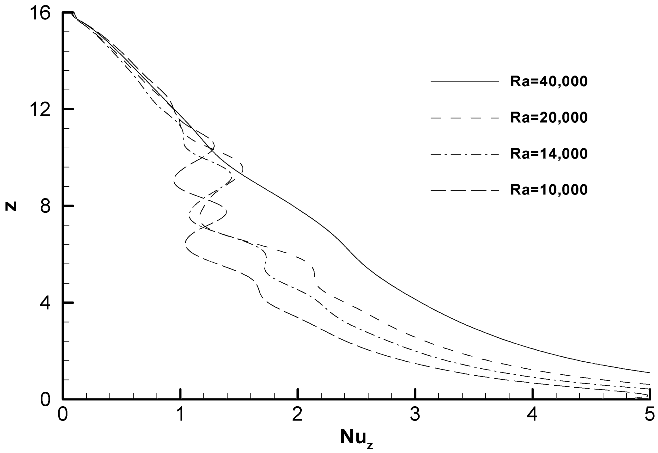

Fig. 10. The local Nusselt numbers along the hot wall for several Ra

The heat transfer across the tall cavity by natural convection is dependent on the flow-pattern. This was found from the wavy distribution of local Nusselt numbers shown in Figure 10 when t = 200.

The result of comparison with experiment is shown in Figure 11. The relevant values are shown in Table 3. Experimental results were given according to the correlations of ElSherbiny et al. A good agreement was found for Rayleigh number less than 100000, beyond which the discrepancy increases with Ra. But the maximum discrepancy at Ra = 600000 is about 18%.

4
Conclusions

Numerical study of the transient laminar natural convection of air in a tall cavity with an aspect ratio of 16 was presented, where the projection method III (PmIII) was implemented in a very fine staggered grid system. The cellular pattern was found merely in case of suddenly heating mode. The number of cells was found to be dominated by Rayleigh number. There are a closed region and an open region of Rayleigh number, in which numerical simulation in terms of PmIII can provide multicellular flow pattern. The two regions are given by

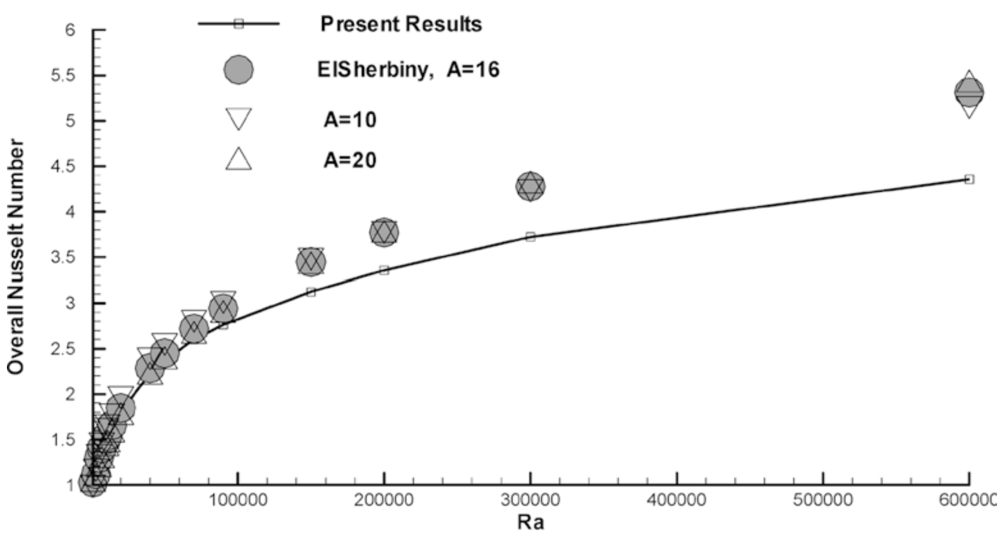

Fig. 11. The comparison between the overall Nusselt numbers from current calculation and the measured results

$Ra \in [7000, 20000]$ and $Ra \geq 118000$. The cell distance appeared at critical Rayleigh number is 2.0 which is coincident with the experimental finding for Bénard problem. However, in the remained region, single central cellular pattern should be emerged. In the open multicellular region of Ra, the overall Nusselt number obtained by numerical simulation has much large deviation from the measured data. However, the maximum deviation for overall Nusselt number from experimental data is less than 6% when $Ra \leq 100000$.

References

1. Ostrach, S.: Natural Convection in Enclosures. ASME J. of Heat Transfer. 110 (1988) 1175–1190
2. Batchelor, G. K.: Heat Transfer by Free Convection Across a Closed Cavity Between Two Vertical Plates with Different Temperatures. Q. Appl. Math. 12 (1954) 209–233
3. Elder, J. W.: Laminar Free Convection in a Vertical Slot. J. Fluid Mech. 23 (1965) 77–98
4. Gill, A. E.: The Boundary Regime for Convection in a Rectangular Cavity. J. Fluid Mech. 26 (1966) 515–536
5. Bejan, A.: Note on Gill's Solution for Free Convection in a Vertical Enclosure. J. Fluid Mech. 90 (1979) 561–568
6. Graebel, W. P.: The Influence of Prandtl Number on Free Convection in a Rectangular Cavity. Int. J. of Heat and Mass Transfer. 24 (1981) 125–131
7. Ostrach, S.; Raghavan, C.: Effect of Stabilizing Thermal Gradients on Natural Convection in Rectangular Enclosure. ASME J. of Heat Transfer. 101 (1979) 238–243
8. ElSherbiny, S. M.; Raithby, G. D.; Hollands, K. G. T.: Heat Transfer by Natural Convection Across Vertical and Inclined Air Layers. ASME J. Heat Transfer. 104 (1982) 96–102
9. Hollands, K. G. T.; Konicek, L.: Experimental Study of the Stability of Differential Heated Inclined Air Layers. Int. J. Heat and Mass Transfer. 16 (1973) 1467–1476
10. Schmidt, R.J.; Milverton, S. W.: On the Stability of a Fluid When Heated from Below. Proc. Roy. Soc. (London) A, 152 (1935) 486–500
11. Wirtz, R. A. Liu, L. H.: Numerical Experiments on the Onset of Layered Convection in a Narrow Slot Containing a Stably Stratified Fluid. Int. J. of Heat and Mass Transfer. 18 (1975) 1299–1305
12. Hart, J. E.: On Sideways Diffusive Instability. J. Fluid Mech. 49 (1971) 279–288
13. Korpela, S. A.; Lee, Yee; Drummond, J. E.: Heat Transfer Through a Double Pane Window. ASME J. Heat Transfer. 104 (1982) 539–544
14. Le Quéré P.: A Note on Multiple and Unsteady Solutions in Two-Dimensional Convection in a Tall Cavity. ASME J. of Heat Transfer. 112 (1990) 965–974
15. Jin, Y. Y.; Chen, C. F.: Instability of Convection and Heat Transfer of High Prandtl Number Fluids in a Vertical Slot. ASME J. of Heat Transfer. 118 (1996) 359–365
16. Wakitani, S.: Experiments on Convective Instability of Large Prandtl Number Fluids in a Vertical Slot. ASME J. Heat Transfer. 116 (1994) 120–126
17. Wakitani, S.: Development of Multicellular Solution in Natural Convection in an Air-Filled Vertical Cavity. ASME J. Heat Transfer. 119 (1996) 97–101
18. Yang, H. X.; Zhu, Z. J.; Gilleard, J.: Numerical Simulation of Thermal Fluid Instability Between Two Horizontal Parallel Plates. Int. J. Heat and Mass Transfer. 44 (2001) 1485–1493
19. Lir, J. T.; Lin, T. F.: Visualization of Roll Patterns in Rayleigh-Bénard Convection of Air in a Rectangular Shallow Cavity. Int. J. Heat and Mass Transfer. 44 (2001) 2889–2902
20. Brown, D. L.; Cortez, R.; Minion, M. L.: Accurate Projection Methods for the Incompressible Navier-Stokes Equations, J. of Comput. Phys., 168 (2001) 464–499
21. Zhu, Z. J.: Numerical Simulation of Flow Around Rectangular Cylinders. Ph.D. Thesis, Shanghai JiaoTong University, 1990
22. Baker, T. J.: Potential Flow Calculation by the Approximate Factorization Method, J. of Comput. Phys., 42 (1981) 1–19
23. Kim, J.; Moin, P.: Application of a fractional-step method to incompressible Navier-Stokes equations, J. of Comput. Phys., 59 (1985) 308
24. Le Quéré P.: Computation of Natural Convection in Two-Dimensional Cavities with Chebyshev Polynomials. J. of Comput. Phys. 57 (1985) 210–228
25. Chandrasekhar, S.: Hydrodynamic and Hydro-magnetic Stability. London: Oxford University Press, 1961